A Stochastic Resonance Electrocardiogram Enhancement Algorithm for Robust QRS Detection

Cihan Berk Güngör, *Student Member, IEEE*, Patrick P. Mercier, *Senior Member, IEEE*, and Hakan Töreyin, *Member, IEEE*

***Abstract*—This study presents a new QRS detection algorithm making use of the background noise that is inevitably present in electrocardiogram (ECG) recordings. The algorithm suppresses noise, enhances the QRS-waves, and applies a threshold for QRS detection. Noise suppression and QRS enhancement are performed by a band-pass filter stage followed by a nonlinear stage based on the interaction of a particle inside an underdamped monostable potential well. The nonlinear stage maximizes the output when there is a QRS-wave and minimizes the output otherwise. One of the instruments that the nonlinear stage uses to enhance the QRS-waves is stochastic resonance, where the output is maximized for a non-zero intensity background noise. In terms of QRS-wave detection $F1$ score, which ranges from 98.87% to 99.99% on four major benchmarking databases (MIT-BIH Arrhythmia, QT, European ST-T, and MIT-BIH Noise Stress Test), the algorithm outperforms all existing ECG processing algorithms. The study, for the first time, demonstrates QRS-enhancement by facilitating stochastic resonance while suppressing in-band noise of ECG signals. Detecting QRS-waves as the ECG data streams, having a complexity of $O(n)$, and not requiring any training data make the algorithm convenient for real-time ECG monitoring applications with limited computational resources.**

***Index Terms*— ECG monitoring, QRS-wave, Stochastic resonance**

I. Introduction

THE electrocardiogram (ECG) represents the electrical activity of heart muscle and thus has significant clinical value in assessing cardiovascular health. ECG allows tracking of heart rate (HR), which has diagnostic and prognostic importance in cardiovascular (e.g., hypertension, coronary artery disease, and cardiomyopathy [1], [2]), autonomic nervous system (ANS) (e.g., diabetic neuropathy, myocardial infarction (MI), and diabetes mellitus [3]–[5]) disorders.

In ECG, HR is obtained by first detecting heart beats from the prominent peaks corresponding to depolarization of the large mass of the ventricles, namely the QRS complex. Then, the time difference between successive QRS-waves is used to identify the instantaneous HR. One of the major challenges of HR detection from ECG arises from the noise in a recording. As classified in [6]–[8], electrode motion artifact, dc swing, and high frequency noise are three common noise and interference types that deteriorate ECG recordings independent of the measurement instrumentation. Electrode motion artifacts are a combination of high and low frequency components (0 to ~20 Hz [8]) originating from movement of a subject or applied mechanical force on the electrodes [6], [8]. Muscle noise occurs at high frequency (20 to 50 Hz [6]) and originates from electrochemical processes in the activated skeletal muscles. DC swing is a low frequency noise [7] that originates from movements of subject or the leads [6], [7]. The bandwidth overlap of these noise and interference sources and the QRS-wave (8 to 50 Hz [9]) makes it challenging to accurately extract the HR in a noisy ECG recording [6].

A common approach for QRS detection is noise suppression followed by a QRS enhancement algorithm. In fact, low-complexity signal-enhancement-based QRS detection algorithms have resulted in detection sensitivity as high as 99.95% [10] and positive predictivity as high as 99.96% [11] on the primary benchmarking database of MIT/BIH arrythmia database [12]. On the other hand, in recordings with larger noise and artifacts, the performance of such algorithms reduce as low as 93.14% in sensitivity and 86.23% in positive predictivity [13], [14]. Additionally, interpatient variation on ECG morphologies also deteriorates the performance [15], [16]. Alternatively, neural network algorithms (e.g., convolutional neural network [17]) can offer better performance in noisy scenarios [15], [17]. However, the performance of a neural network is highly data dependent. Therefore, to reflect the wide spectrum of QRS waveform shapes and background noise and artifact conditions, diverse training datasets are needed [15]–[17].

The paper was submitted on November 26, 2021 for review. This material is based upon work supported by the National Science Foundation under Grant Number 1916160.

C. B. Güngör is with the Department of Electrical and Computer Engineering, University of California at San Diego, La Jolla, CA 92093 USA and with the Department of Electrical and Computer Engineering, San Diego State University, San Diego, CA 92182 USA (e-mail: cgungor@ucsd.edu).

P. P. Mercier is with the Department of Electrical and Computer Engineering, University of California at San Diego, La Jolla, CA 92093 USA (e-mail: pmercier@ucsd.edu).

H. Töreyin is with the Electrical and Computer Engineering Department, San Diego State University, San Diego, CA 92182 USA, (e-mail: htoreyin@sdsu.edu).

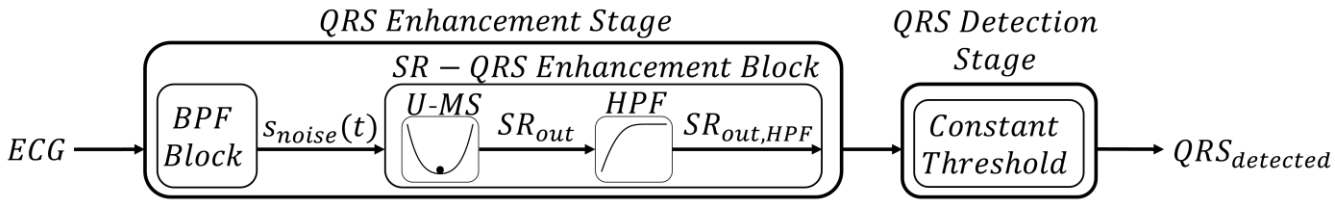

Fig. 1. Block diagram of the proposed QRS detection algorithm.

Algorithm 1 Complete QRS-Wave Detection Algorithm

Input: $s_{ECG}(t)$ (ECG signal)
Output: $QRS_{detected}, Se, +P, F1, DER, Acc$ (Performance metrics and QRS-wave locations)

1 $s_{noise}(t) \leftarrow BPF(s_{ECG}(t))$ # ECG signal is band pass filtered
2 $h_{opt}, a_{opt}, b_{opt}, \gamma_{opt}, d_{th_{opt}} \leftarrow PS(s_{noise}(t))$ # Parameter selection
3 $x(t) \leftarrow SR\left(s_{noise}(t), h_{opt}, a_{opt}, b_{opt}, \gamma_{opt}, d_{th_{opt}}\right)$ # SR with optimal parameters
4 $s_{out,HPF}(t) \leftarrow HPF(x(t))$ # SR output is high pass filtered
5 $QRS_{detected} \leftarrow TH(s_{out,HPF}(t))$ # Constant threshold is applied to obtain output QRS locations
6 $TP, FN, FP \leftarrow PM(QRS_{detected}, QRS_{true})$ # Performance metrics are obtained
7 $Se, +P, F1, DER, Acc \leftarrow DP(TP, FN, FP)$ # Detection performance is obtained

Notably, additive noise in a signal – counterintuitively – can potentially be used for signal enhancement, a phenomenon named as stochastic resonance (SR) [18]. In fact, various systems with nonlinear dynamics (e.g., rotating machine bearing [19], [20], underwater acoustic communication [21], information transmission in neural networks [22], and eye movement desensitization [23]) make use of noise on the signal and/or in the system to improve detection of weak signals below the detection threshold. In a system facilitating SR, there is an optimal level of noise intensity that maximizes the signal power and/or detectability [18], [24]–[26].

Motivated by the low-complexities of signal-enhancement-based QRS detection methods and high performances of previous signal enhancement and detection methods facilitating SR [19], [25], a novel low-complexity QRS detection algorithm is proposed and investigated in this study. The algorithm consists of a QRS enhancement and a QRS detection stage. The core of the QRS enhancement stage is an innovative SR-QRS enhancement block that acts as a nonlinear filter that facilitates SR. The block makes use of the inevitable additive noise of ECG to enhance QRS-waves while suppressing the noise outside the QRS-wave regions. Additionally, two unique properties make the proposed algorithm appropriate for real-time ECG monitoring applications with limited computational resources. First, the algorithm does not necessitate a reverse search step and thus detects QRS-waves as the data streams through. Second, the algorithm does not need any training data for parameter optimization. The algorithm is implemented using MATLAB (MathWorks, Natick, MA, USA) and provided at "https://github.com/cihanbgungor/SR_QRS_detector".

The rest of the paper is organized as follows. In Section II, the proposed QRS detection algorithm and the benchmarking datasets are presented. The results are presented in Section III, which are followed by a discussion in Section IV. The paper is concluded in Section V.

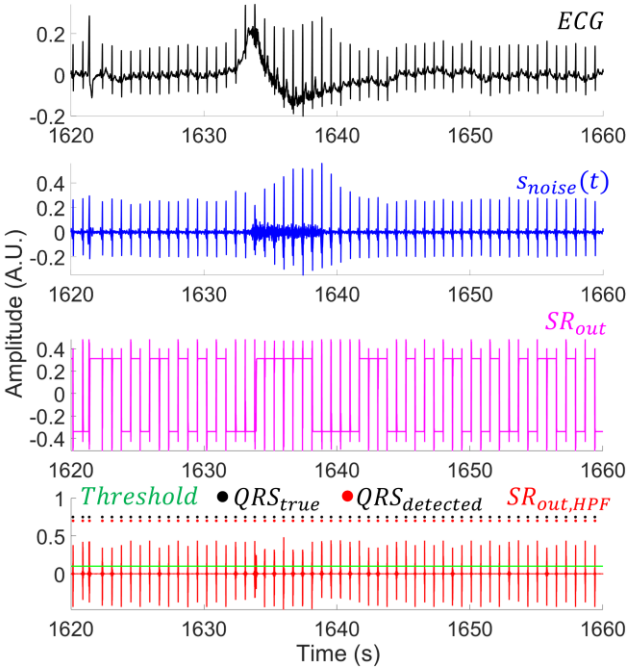

Fig. 2. Exemplary ECG signal (#116 of the MIT-BIH Arrhythmia database) and waveforms within the signal processing chain. For signal labels refer to the block diagram in Fig. 1. The constant threshold level, true (QRS_{true}) and detected ($QRS_{detected}$) QRS-waves are given in the bottom sub-plot.

II. Methods

A. Proposed QRS Detection Algorithm

The proposed QRS detection algorithm consists of a QRS enhancement stage followed by a QRS detection stage as shown in Fig. 1. The pseudocode of the algorithm is presented in Algorithm 1. The QRS enhancement stage amplifies the QRS-waves while suppressing noise. The out-of-band noise is suppressed by a standard band-pass filter (BPF) block implemented as a 4th order finite impulse response (FIR) filter with cutoffs of 0.05 and 100 Hz. (Line 1 of Algorithm 1). Following parameter selection (Line 2 of Algorithm 1), the in-band noise suppression and SR-QRS amplification are achieved by the SR-QRS enhancement block (Lines 3 and 4 of Algorithm 1), which is detailed below in Section II.B. The QRS detection stage consists of a constant thresholding block (Line 5 of Algorithm 1), which is presented in Section II.C. Finally, the performance metrics are obtained (Lines 6 and 7 of Algorithm 1). A 40 s portion of an example ECG recording (# 116) from the MIT-BIH Arrhythmia database [12] and the corresponding waveforms along the signal processing chain of the proposed algorithm are presented in Fig. 2. The hard threshold level, as

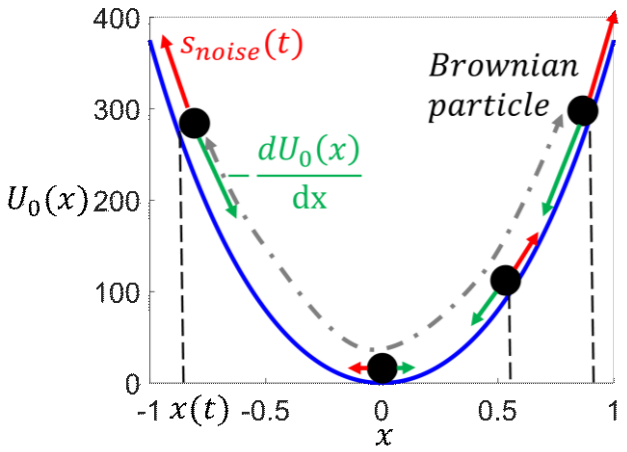

Fig. 3. Stochastic resonance (SR) illustration in a monostable well. Two forces ($s_{noise}(t)$ and $-\frac{dU_0(x)}{dx}$) acting upon the particle are shown on different points of the monostable well.

well as true (QRS_{true}) and detected ($QRS_{detected}$) QRS-waves are shown on the output of the SR-QRS enhancement block.

B. SR-QRS Enhancement Block

Stochastic resonance (SR) describes signal enhancement by exploiting additive noise [18], [25]. This counterintuitive performance improvement of noise necessitates a nonlinear system, which allows complex interactions among the system and noise [27]. Signal improvement exhibits itself in various forms from signal-to-noise ratio (SNR) improvement [25], [26], [28] to signal transmission [27], [29], [30].

A classical nonlinear system used to facilitate SR for weak signal enhancement is an overdamped particle inside a one-dimensional symmetric double well potential [18], [25]. Different damping and well potential shape combinations also exhibit SR for non-periodic signals such as neural spikes [31], [32], bearing faults [19], [20], and acoustic signals [21]. Notably, our investigation of an extracellular neural spike detection algorithm based on SR facilitation using a monostable well with adaptive damping control demonstrates an SNR increase as large as 92 dB [32].

Motivated by our previous nonlinear filter system that results in high SNR improvement [32], we design an SR-QRS enhancement block for the proposed QRS detection algorithm. Specifically, the SR-QRS enhancement block consists of an underdamped particle in a monostable well (U-MS) with adaptive damping control followed by a high-pass filter (HPF). The sub-sections 1 through 4 below present the details of the underdamped particle in a monostable well (U-MS) and the sub-section 5 presents the HPF details.

1) Underdamped Brownian particle in a monostable potential well (U-MS)

The core of the SR-QRS enhancement block is a nonlinear filter modeling the dynamics of a particle in a monostable well described by a function of $U_0(x)$ (Fig. 3).

Here, the band-pass filtered ECG recording, $s_{noise}(t)$, is applied as a time-varying force (Fig. 3) acting on the particle. Notably, $s_{noise}(t)$, is a linear combination of the noise-free ECG signal, $s(t)$, and undesired in-band noise (e.g., electrode motion artifact, high-frequency noise, dc swing), $n(t)$:

$$s_{noise}(t) = s(t) + n(t). \quad (1)$$

In (1), the prominent features of $s(t)$ have deterministic characteristics owing to the physiological limits (e.g., QRS-waves are high amplitude and short duration features). On the other hand, $n(t)$ exhibits stochastic characteristics. As such, the stochastic $n(t)$ causes the particle to exhibit the pattern of motion of a Brownian particle, namely random small fluctuations. Accordingly, the particle in such a system is named as a Brownian particle.

The second force on the Brownian particle is proportional to the slope of the monostable well and denoted as $-\frac{dU_0(x)}{dx}$.

The motion of the Brownian particle inside an underdamped monostable potential well described by $U_0(x)$, is governed by the generalized Langevin equation [33], [34], which takes the form [25]:

$$\frac{d^2x(t)}{dt^2} + \gamma\frac{dx(t)}{dt} = -\frac{dU_0(x)}{dx} + s_{noise}(t), \quad (2)$$

where $x(t)$ is the Brownian particle position and γ is the damping factor. Specifically, (2) describes the dependence of the acceleration and velocity of the particle (left-hand side) on the two forces acting on the particle (right-hand side). The monostable well potential and its derivative for the dimension x are described as:

$$U_0(x) = \frac{ax^2}{2} + \frac{bx^4}{4}. \quad a, b > 0 \quad (3)$$

$$\frac{dU_0(x)}{dx} = ax + bx^3. \quad a, b > 0 \quad (4)$$

where a and b are the well parameters that control stable point depth and wall slope.

For the system governed by the equations (1) through (4), the input is $s_{noise}(t)$ and the output is the particle position, $x(t)$. Therefore, noise suppression of the system translates into restriction of the particle movement when the input is noise, whereas QRS enhancement corresponds to large displacement of the particle during QRS portions. It is noteworthy that with the goal of detecting QRS-waves in this paper, the definition of noise is extended to include all noisy ECG portions except the QRS-wave segments. Although such ECG portions include other physiologically important ECG features (e.g., P-wave and T-wave), they are undesired from QRS-wave detection perspective.

The following sub-section, Section II.B.2, provides details about how the nonlinear U-MS system performs in-band noise suppression and facilitates SR for QRS enhancement.

2) U-MS in-band noise suppression and QRS enhancement

Two factors, namely small $s_{noise}(t)$ and large γ, collectively limit the particle movement and thus suppress the in-band noise. First, $s_{noise}(t)$ amplitude is smaller in noise portions compared to the QRS-wave segments. Therefore, in those portions, the particle in Fig. 3 is primarily under the influence of $n(t)$ and $-\frac{dU_0(x)}{dx}$, and thus swings within a proximity around the stable point. Second, for small $s_{noise}(t)$ amplitudes, the damping in the system is adjusted as high (i.e., γ is large), which further limits the particle movement.

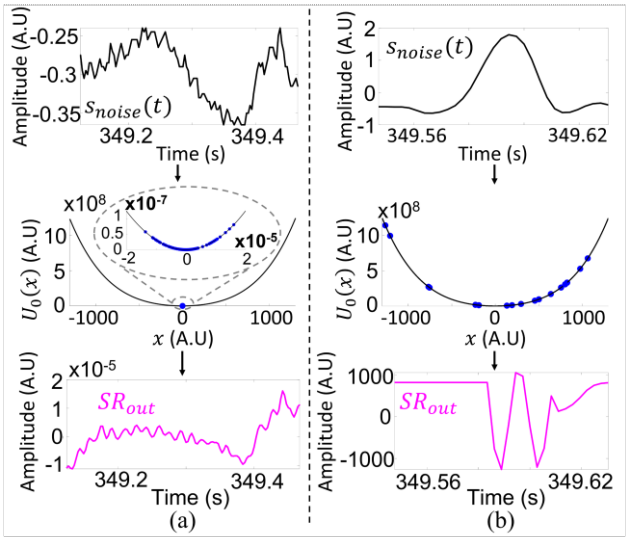

Fig. 4. In-band noise suppression and QRS enhancement are demonstrated on example (a) noise-only and (b) QRS-wave portions. For both columns, top and bottom rows respectively show the input and output signals of the U-MS sub-block of the SR-QRS enhancement block. Middle rows show the positions of the particle for all time steps. A zoomed-in version of the particle positions confined in a small region in (a) are displayed in the inset.

Three factors; namely large $s_{noise}(t)$, small γ, and stochastic resonance; jointly result in large displacement of the particle during the QRS portions of the ECG recording and thus QRS enhancement. First, QRS-wave portions of the ECG signal apply sufficiently large $s_{noise}(t)$ force to push the particle away from the stable point towards the walls of the potential well. Second, to maximize both signal enhancement and noise suppression, the system adapts a dynamic adjustment of the damping coefficient, γ, depending on the input signal amplitude: For good noise suppression, γ is increased when $s_{noise}(t)$ is small; whereas for good QRS enhancement, γ is reduced when $s_{noise}(t)$ is large. Specifically, the damping factor is adjusted to $\gamma = 120$ for the range of input amplitude $s_{noise}(t) < \frac{s_{noise,pp}}{d_{th}}$ and $\gamma = 0.12$ for $s_{noise}(t) \geq \frac{s_{noise,pp}}{d_{th}}$ where $s_{noise,pp}$ is the peak-to-peak value of the entire recording and $d_{th} = 10$ is the damping factor threshold. Third, an optimum intensity of the additive stochastic $n(t)$ causes QRS-enhancement by facilitating stochastic resonance. To understand, a QRS-wave portion without and with $n(t)$ can be considered. In a hypothetical scenario of $n(t) = 0$, the particle moves away from the stable point solely by the force exerted by the QRS-wave. In a practical non-zero $n(t)$ case, the $n(t)$ increases the force exerted by the QRS-wave and thus assists the particle displacement, thereby enhancing the output. Here, the noise intensity is critical: Small noise intensities would not be sufficient to displace the particle any further, whereas higher noise densities would swamp the QRS-wave. A probabilistic investigation of the system using the Fokker-Planck equation to characterize the noise-dependent space-time probability density function of the Brownian particle is beyond the scope of this study. However, readers are referred to [35] for such an analysis for a similar system.

The in-band noise suppression is demonstrated in Fig. 4 (a), where for a noise-only portion with a peak-to-peak value of 0.12 (top row), the positions of the particle at different time steps are shown with blue dots (middle row). As seen at the bottom row, the small amplitude $s_{noise}(t)$ and the high damping coefficient of $\gamma = 120$ limit the peak-to-peak output to 2.8×10^{-5} (73 dB noise suppression). Additionally, the role of dynamic damping adjustment in improving the noise suppression is illustrated in Fig. 5. For the same input, in contrast to an output noise peak-to-peak value of 0.2 obtained when γ is static, the dynamic adjustment results in an output noise peak-to-peak value of 10^{-3}. The in-band noise suppression performance is assessed on three ECG recordings from the MIT-BIH Arrhythmia database [12]. For low- (# 103), medium- (# 116), and high-noise (# 207) recordings, the ECG in-band ([0.05 Hz-100 Hz]) noise power suppression of the SR-QRS Enhancement Block are respectively found as 85.6 dB, 82.68 dB, and 72.33 dB.

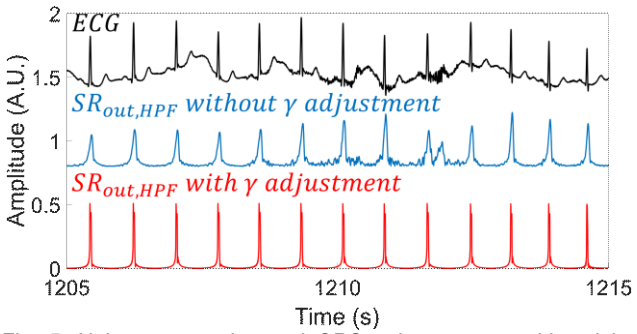

Fig. 5. Noise suppression and QRS enhancement achieved by adaptive adjustment of damping coefficient, γ.

QRS-enhancement by the U-MS is demonstrated in Fig. 4(b), where for a large $s_{noise}(t)$ due to a QRS-wave, the force exerted onto the particle is large and the damping coefficient is small ($\gamma = 0.12$), thereby allowing the particle to escape from the stable point and enhancing the signal. For a QRS-wave with a peak-to-peak value of ~2.4, the output has a peak-to-peak value of ~2200. QRS-enhancement is also demonstrated in Fig. 5 as the large peaks at the output that are synchronized with the QRS-waves of the input. Facilitation of stochastic resonance in QRS enhancement is demonstrated in Fig. 6 in the Section III. In Fig. 6, ΔSNR peaks for a non-zero noise intensity for different noise types.

3) Numerical solution of the U-MS

The solution of (2), $x(t)$, can be approximated by an iterative numerical method, namely the fourth-order Runge-Kutta (RK) method [25], [36]:

$$x[n+1] = x[n] + (p_1 + 2p_2 + 2p_3 + p_4)h/6, \quad (5)$$
$$y[n+1] = y[n] + (k_1 + 2k_2 + 2k_3 + k_4)h/6, \quad (6)$$

where $x[n]$ is the n^{th} sample of $x(t)$, $y[n]$ is the n^{th} sample of $\frac{dx(t)}{dt}$, and h is the step size of the RK approximation. The pseudocode of the solution, k_1 through k_4, and p_1 through p_4 are provided in the pseudocode, Algorithm 2.

4) Parameter selection of the U-MS

Parametric search of well and solver parameters (i.e., a, b, h, γ, d_{th}) is performed to optimize QRS enhancement. The search is conducted without the need for *a priori* knowledge of

Algorithm 2 *SR* - QRS Enhancement Block - Numerical Solution

Input: $s_{noise}(t), h, a, b, \gamma, d_{th}$ (Band pass filtered ECG signal and parameters)
Output: $x(t)$ (Output signal)

$x(1) \leftarrow 0$ # Initial value to $x(t)$ is set
$y(1) \leftarrow 0$ # Initial value to $y(t)$ is set
$s_{noise,pp} \leftarrow \max(s_{noise}(t)) - \min(s_{noise}(t))$ # Signal peak-to-peak amplitude is set

for ($i = 1$ to $length(s_{noise}(t)) - 1$) **do**
  if ($s_{noise}(i) < s_{noise,pp}/d_{th}$) **then**
    $\gamma \leftarrow \gamma * 10$ # Damping coefficient is increased for low amplitude samples of the signal
  else
    $\gamma \leftarrow \gamma/100$ # Damping coefficient is reduced for high amplitude samples of the signal
  end if
  $p_1 \leftarrow y(i)$
  $k_1 \leftarrow -a * x(i) - b * x(i)^3 - \gamma p_1 + s_{noise}(i)$
  $p_2 \leftarrow y(i) + k_1 * h/2$
  $k_2 \leftarrow -a * (x(i) + p_1 * h/2) - b * (x(i) * p_1 * h/2)^3 - \gamma p_2 + s_{noise}(i)$
  $p_3 \leftarrow y(i) + k_2 * h/2$
  $k_3 \leftarrow -a * (x[i] + p_2 * h/2) - b * (x(i) * p_2 * h/2)^3 - \gamma p_3 + s_{noise}(i+1)$
  $p_4 \leftarrow y(i) + k_3 * h$
  $k_4 \leftarrow -a * (x(i) + p_3 * h) - b * (x(i) * p_3 * h)^3 - \gamma p_4 + s_{noise}(i+1)$
  $x(i+1) \leftarrow x(i) + (p_1 + 2 * p_2 + 2 * p_3 + p_4) * h/6$ # The next $x(\cdot)$ is obtained from the calculated slopes
  $y(i+1) \leftarrow y(i) + (k_1 + 2 * k_2 + 2 * k_3 + k_4) * h/6$ # The next $y(\cdot)$ is obtained from the calculated slopes
end for
return $x(t)$

the true QRS locations, QRS_{true}. The optimization aims to maximize the output SNR defined as:

$$SNR = 20log\left(\frac{A_{pp\ of\ QRS-wave}}{Standard\ deviation\ of\ a\ noise\ segment}\right), \quad (7)$$

where A_{pp} is the average peak-to-peak amplitude of 100 arbitrarily selected QRS-waves. QRS regions are segmented as 100 ms time windows centered around the detected QRS-wave points, $QRS_{detected}$. The 100 $QRS_{detected}$ point set consists of one automatically and arbitrarily selected $QRS_{detected}$ point using the $rand$ function of MATLAB and the 99 $QRS_{detected}$ points succeeding it. A total of 100 noise segments (~1 s each) are selected arbitrarily inside the sections between the selected 100 QRS segments.

The selection of the well/solver parameter values is conducted through a three-step parametric search maximizing the SNR improvement of the system defined as $\Delta SNR = SNR_{out} - SNR_{in}$; where SNR_{out} and SNR_{in} are respectively the SNR of the output and input signals. The three steps consist of (1) initialization of the parameters, (2) forward parametric search, and (3) reverse parametric search. The forward parametric search order is in the direction that parameter specificity increases. The parameters that affect the most characteristics of the system and the solution are optimized first. Therefore, the first parameter that is optimized is the h parameter, which defines the step size of the RK solver and thus affects the whole solution regardless of where the particle is inside the well. Then, a and b parameters that describe the well properties altogether (e.g., curvature, depth, steepness) are optimized. The damping of the system is different depending on the input signal amplitude and thus is an input-specific behavior of the system. The two parameters, γ and d_{th}, define the damping behavior and thus these parameters are optimized the last. The forward parametric search follows the order of $h \rightarrow a \rightarrow b \rightarrow \gamma \rightarrow d_{th}$ and the reverse parametric search follows the order of $\gamma \rightarrow b \rightarrow a \rightarrow h$.

At the initialization step, well/solver parameters are initialized with values as follows [31], [32]: $h_0 = 40$, $a_0 = -1000$, $b_0 = 1$, $\gamma_0 = 1$, $d_{th,0} = 2$. Notably, the numerical solution of (2) diverges when a parameter value is arbitrarily increased/decreased from the initial value, thereby causing MATLAB to halt. For a time-efficient search that minimizes the search time, the search of a parameter is carried out in multiple non-overlapping search windows with identical length. Specifically, the initial search window is shifted in the positive and negative directions by an amount equal to the window length until the output diverges in the new search window. In each search round, the parameter value that locally maximizes the SNR is found via a 50-step sweep. Finally, the local maxima of all search rounds are compared to find the parameter value of the global maximum. The search window length, p_{window}, for a parameter p, where $p \in \{a, b, h, \gamma, d_{th}\}$, is set at the initial search step as $p_{window} = p_{up} - p_{low}$. Here, p_{up} and p_{low} are respectively the upper and the lower boundaries of the initial search window and are selected such that they satisfy $\left|SNR|_{p_{up(low)}} - SNR|_{p_0}\right| = 3\ dB$.

5) High-pass filter

While adaptive adjustment of the damping coefficient based on the input signal amplitude improves in-band noise suppression performance, it also introduces a minor change to the system response. Increasing the damping in small-amplitude portions of the signal that immediately follows a large amplitude QRS-wave causes the particle to move around a new x location, thereby resulting in a bistable behavior as seen in the 3rd row of Fig. 2. Using a 4th order FIR high-pass-filter with a cutoff frequency of 10 Hz, the bistable behavior is eliminated (Fig. 2 – 4th row, red waveform) before the signal is fed to the QRS-Detection stage.

C. QRS-Detection Stage

A constant threshold of 0.1 is applied on the QRS-enhancement stage output to determine the QRS-waves, $QRS_{detected}$. In the binary output of the threshold stage, the time instances corresponding to the data points at the center of a *'0'*-to-*'1'* transition followed by a *'1'*-to-*'0'* transition are identified as the $QRS_{detected}$. Based on the identified QRS-waves, the performance metrics, $TP, FN,$ and FP are obtained by comparing the locations of the $QRS_{detected}$ with true QRS-waves, QRS_{true}, obtained from database annotations. For each $QRS_{detected}$, QRS_{true} is searched within a ±150 ms time window centered around QRS_{true} following ANSI/AAML EC38 [37] and EC57 [38] and studies in [39]–[42]. A $QRS_{detected}$ inside a search window is counted as a true positive, TP. The search windows with no $QRS_{detected}$ are counted as false negatives, FN. The number of false positives, FP, is calculated as the difference of the number of $QRS_{detected}$

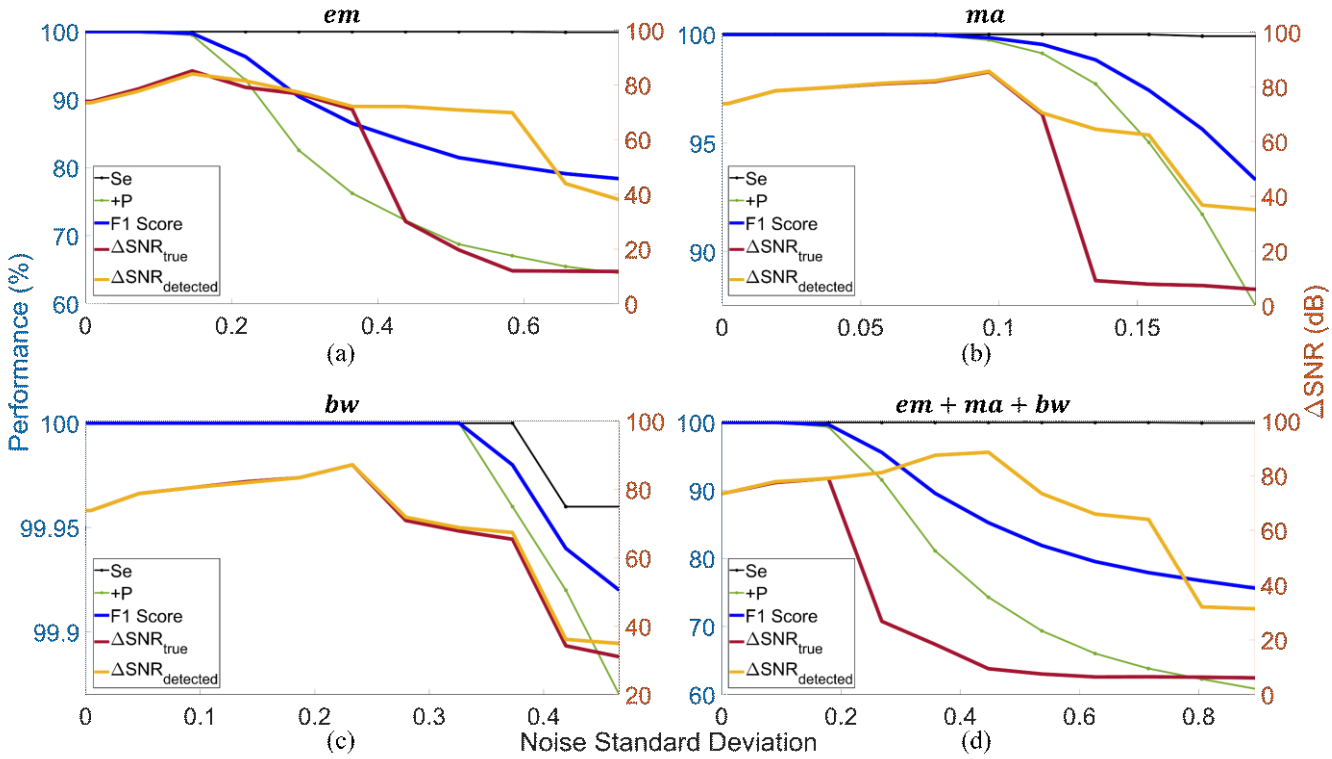

Fig. 6. QRS enhancement (right y-axes) and QRS detection (left y-axes) performance results of the proposed algorithm when (a) em noise, (b) ma noise, (c) bw noise, and (d) $em + ma + bw$ is added to ECG signal as in (9). QRS enhancement results are given in ΔSNR_{true} and $\Delta SNR_{detected}$, which respectively correspond to ΔSNR calculated using QRS_{true} and $QRS_{detected}$.

TABLE I
CHARACTERISTICS OF THE PUBLICLY AVAILABLE DATABASES USED FOR VALIDATION

Database	# of recordings	f_s (Hz)	Recording duration (min)	Total # of beats
MIT-BIH Arrhythmia	48	360	30	109518
MIT-BIH NST	12	360	30	25590
QT	105	250	15	87708
EDB	90	250	120	790558

and TP.

Based on TP, FN, and FP; detection performance is evaluated by five metrics, namely sensitivity (Se), positive predictivity ($+P$), F1 score ($F1$), detection error rate (DER), and accuracy (Acc) given as:

$$Se\ (\%) = \frac{TP}{TP+FN} * 100,\ +P\ (\%) = \frac{TP}{TP+FP} * 100,$$
$$F1\ (\%) = \frac{2*Se*(+P)}{Se+(+P)}, \quad (8)$$
$$DER\ (\%) = \frac{FP+FN}{TP} * 100,\ Acc\ (\%) = \frac{TP}{TP+FN+FP} * 100.$$

D. Datasets

The algorithm is initially assessed in terms of how different noise intensities affect the QRS enhancement and QRS detection performance. Accordingly, the noise recordings (i.e., em, ma, and bw) in the MIT/BIH NST database [6] are used to vary the noise intensity in a controlled manner. In [6], em, ma, and bw correspond to electrode motion artifact, muscle artifact, and baseline wander, respectively. Specifically, recordings with different noise intensities, $s_{noise}(t)$, are obtained via linear summation of a low noise ECG signal (recording 100 of the MIT-BIH Arrhythmia database [12]), $s(t)$, with the noise recording, $n(t)$, weighed by a noise intensity factor, g, as follows:

$$s_{noise}(t) = s(t) + g * n(t). \quad (9)$$

Additionally, the QRS-wave detection performance of the proposed algorithm is evaluated using the standard benchmarking datasets of the MIT-BIH Arrythmia [12], QT [43], European ST-T (EDB) [44], and MIT-BIH Noise Stress Test (NST) [6] databases. The major features of these databases (i.e., number of recordings, recording length, and total number of beats) are provided in Table I.

III. RESULTS

QRS enhancement performance of the proposed algorithm is first analyzed for different noise intensities for each noise type in the MIT-BIH NST database; namely em, ma, and bw. Specifically, the SNR improvements for a range of noise standard deviations are obtained by sweeping g in (9) for each noise type. The noise standard deviation is increased until the output SNR drops to below 40 dB. For each g value of the input, $s_{noise}(t)$, having an SNR of SNR_{in}, the algorithm is optimized separately to obtain the largest output SNR, SNR_{out} following the procedure described in Section II.B.4. SNR improvement is calculated as $\Delta SNR = SNR_{out} - SNR_{in}$. Variation of ΔSNR with noise standard deviation for each of the three noise types and the combined noise obtained as $n(t) = em + ma + bw$ are as shown in Fig. 6. It is noteworthy that Fig. 6 shows two different ΔSNR calculated using (7): ΔSNR_{true} and $\Delta SNR_{detected}$ respectively correspond to ΔSNR calculated

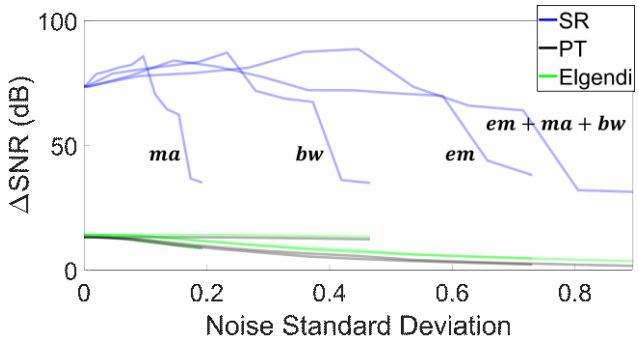

Fig. 7. QRS enhancement (ΔSNR) for the proposed algorithm, PT, and Elgendi algorithms when all noise types (em, ma, bw, and $em + ma + bw$) are added to ECG signal as in (9).

TABLE II
QRS DETECTION PERFORMANCE EVALUATION OF THE PROPOSED ALGORITHM ON THE MIT-BIH ARRHYTHMIA DATABASE

ECG record #	*Total # of beats*	*Se (%)*	*+P (%)*	*DER*	*Acc (%)*
105	2572	99.96	100	0.039	99.96
107	2137	99.96	100	0.046	99.96
108	1774	99.95	100	0.056	99.95
109	2532	99.96	100	0.039	99.96
111	2124	99.95	100	0.047	99.9
116	2412	99.42	100	0.58	99.42
121	1863	99.89	100	0.1	99.89
201	1963	99.95	100	0.05	99.95
203	2980	99.83	100	0.168	99.83
205	2657	99.93	100	0.075	99.93
207	1860	99.25	98.2	2.6	97.47
208	2955	99.66	100	0.34	99.66
217	2208	99.9	100	0.09	99.9
228	2053	99.86	100	0.14	99.86
233	3079	99.97	100	0.03	99.97
Remaining	74349	100	100	0	100
Overall	**109518**	**99.95**	**99.96**	**0.09**	**99.91**

using QRS_{true} and $QRS_{detected}$. In addition to the investigation of how *SNR* changes with noise intensity, the proposed algorithm is also evaluated in terms of how QRS detection performance changes with the noise. For the same algorithm parameters optimized to maximize $\Delta SNR_{detected}$, QRS detection performances are obtained following the procedure explained in Section II.C. For the three noise types, *Se*, *+P*, and *F1* score metrics obtained for each g are presented in Fig. 6 (a)-(c). The results for the combined noise of $n(t) = em + ma + bw$ are presented in Fig. 6 (d). A closer look into the Fig. 6 reveals that, for all noise cases, for even high noise levels, Se remains greater than 99.92, whereas $+P$ and $F1$ dampen with increasing noise levels. A decrease in ΔSNR_{true} with noise intensity is expected to increase FPs. In fact, for the noise types ma, bw and $em + ma + bw$; for noise standard deviations that are respectively greater than ~0.1, ~0.33, and ~0.2; ΔSNR_{true}, $+P$, and $F1$ start decreasing. However, it should also be considered that, as noise intensity increases, the SR-QRS enhancement block can erroneously enhance noise portions as well as the true QRS-waves, which would cause ΔSNR_{true} to remain high while increasing FPs. As a matter of fact, for em, the $+P$ and $F1$ decrease when noise exceeds ~0.15; whereas the $\Delta SNR_{true} >\sim 71\ dB$ for noise levels up to ~0.37. Notably, the discussion above cannot be generalized for

TABLE III
QRS DETECTION COMPARISON ON MIT-BIH ARRHYTHMIA DATABASE

	QRS detection method	**Se (%)**	**+P (%)**
This work	***Stochastic Resonance***	***99.95***	***99.96***
Martinez, 2004 [50]	Wavelet Transform (WT)	99.80	99.86
Martinez, 2010 [11]	Phasor Transform	99.69	99.96
Ghaffari, 2009 [51]	Discrete WT (DWT)	99.91	99.88
Nayak, 2019 [10]	DFOD + SE + HT	99.95	99.94
Burguera, 2019 [60]	Smoothing and PVD	99.57	99.37
Chen, 2020 [63]	HC and DWT	99.89	99.94
Merah, 2015 [14]	Stationary WT (SWT)	99.84	99.88
Modak, 2021 [64]	MAF + TAT	99.82	99.88
Rahul, 2021 [52]	Third power + AT	99.81	99.85
Jia, 2020 [15]	CNN	99.89	99.90
Xiang, 2018 [62] [1]	CNN	99.77	99.91
Chandra, 2019 [39]	CNN	99.84	99.95
Zahid, 2022 [58]	CNN	99.85	99.82
Cai, 2020 [40]	CNN	99.95	99.94
Hossain, 2019 [59]	CEEMD	*99.96*	99.89
Tueche, 2021 [53]	PT-based	99.65	99.69
Peimankar, 2021 [54]	CNN-LSTM	99.61	99.52
Xiong, 2021 [55]	Energy Segmentation	99.36	99.78
Rahul, 2021b [56]	Third power + AT	99.82	99.85
Pander, 2022 [41]	FCMC	99.82	99.88
Lee, 2022 [57]	EMD	99.83	99.92
Yakut, 2018 [69]	PT-based	99.83	99.83

[1] Excludes recordings 102 & 104. DFOD: Digital Fractional Order Differentiator, SE: Shannon Energy, HT: Hilbert Transform, PVD: Peak-Valley Detector, HC: Hierarchical Clustering, MAF: Moving Average Filter, TAT: Time/Amplitude Threshold, AT: Adaptive Thresholding, CEEMD: Complete Ensemble Empirical Mode Decomposition, LSTM: Long short-term memory, FCMC: Fuzzy c-median Clustering, EMD: Empirical Mode Decomposition.

$\Delta SNR_{detected}$, which is calculated using the $QRS_{detected}$, some of which are FPs.

It should be noted that, the essence of the proposed algorithm is QRS detection following QRS enhancement. Therefore, the SNR improvement is compared with the state-of-the-art QRS detection algorithms that perform QRS enhancement prior to detection, namely Pan-Tompkins (PT) [45] and Elgendi [46]. These algorithms are implemented using the MATLAB codes provided in [47] and [48], respectively. The comparison is performed for all noise types and presented in Fig. 7, where ΔSNR difference between the proposed algorithm and the other two ranges from 21.6 dB for the bw noise to 82.91 dB for the combined $em + ma + bw$ noise. Notably, for all noise types, the proposed algorithm offers significantly better ΔSNR than the PT and Elgendi methods.

Following the investigation of the effect of noise on QRS enhancement and detection, the detection performance of the algorithm is assessed on a wide range of ECG morphologies using publicly available benchmarking databases, namely MIT-BIH Arrhythmia, QT, and EDB:

QRS-wave detection performance of the proposed algorithm on the MIT-BIH Arrhythmia database is presented in Table II. In Table II, the recordings with non-zero DER are presented individually, while the remaining recordings are grouped at the last row. The average *Se* and *+P* values for the database are 99.95% and 99.96%, respectively. A further investigation on FPs and FNs on recordings with high DER ($DER > 0.2$) reveals that, right bundle branch block (RBBB) beats are responsible from 95% of all FPs (36 FPs), whereas left bundle branch block (LBBB) beats are responsible from 53.3% of all

TABLE IV
QRS DETECTION COMPARISON ON THE QT DATABASE

	QRS detection method	Se (%)	+P (%)
This work	***Stochastic Resonance***	***99.99***	***99.99***
Martinez, 2004 [50]	Wavelet Transform (WT)	99.92	99.88
Martinez, 2010 [11]	Phasor Transform	99.95	99.93
Ghaffari, 2009 [51]	Discrete WT (DWT)	99.94	99.91
Nayak, 2019 [10]	DFOD + SE + HT	99.95	99.98
Burguera, 2019 [60]	Smoothing and PVD	99.89	99.99
Chen, 2020 [63]	HC and DWT	99.92	99.96
Merah, 2015 [14]	Stationary WT	99.94	99.89
Cai, 2020 [40]	CNN	99.97	99.99
Hossain, 2019 [59]	CEEMD	99.97	99.93
Rahul, 2021 [52]	Third power + AT	99.9	99.94
Peimankar, 2021 [54]	CNN-LSTM	99.7	99.19
Pander, 2022 [41]	FCMC	99.91	99.93
Lee, 2022 [57]	EMD	99.99	99.98

DFOD: Digital Fractional Order Differentiator, SE: Shannon Energy, HT: Hilbert Transform, PVD: Peak-Valley Detector, HC: Hierarchical Clustering, CEEMD: Complete Ensemble Empirical Mode Decomposition, AT: Adaptive Thresholding, LSTM: Long short-term memory, FCMC: Fuzzy c-median Clustering, EMD: Empirical Mode Decomposition.

TABLE V
QRS DETECTION COMPARISON ON THE EDB

	QRS detection method	Se (%)	+P (%)
This work	***Stochastic Resonance***	***99.93***	***99.97***
Martinez, 2004 [50]	Wavelet Transform (WT)	99.61	99.48
Martinez, 2010 [11]	Phasor Transform	99.67	99.73
Ghaffari, 2009 [51]	Discrete WT (DWT)	99.63	99.55
Nayak, 2019 [10]	DFOD + SE + HT	99.87	99.86
Burguera, 2019 [60]	Smoothing and PVD	99.88	*99.98*
Xiong, 2021 [55]	Energy Segmentation	99.77	99.65
Rahul, 2021b [56]	Third power + AT	99.71	99.8
Pander, 2022 [41]	FCMC	99.67	99.86

DFOD: Digital Fractional Order Differentiator, SE: Shannon Energy, HT: Hilbert Transform, PVD: Peak-Valley Detector, AT: Adaptive Thresholding, FCMC: Fuzzy c-median Clustering.

FNs (32 FNs). Of the remaining FNs, 30% originate from normal beats, whereas premature ventricular contractions (PVCs) and the RBBB are responsible from the remaining 16.7%. Notably, the wide S-features of the RBBB merge with the T-waves, which are erroneously enhanced and detected as QRS-waves by the algorithm. In LBBB, the wide QRS-wave with faint Q and S features merge with the T-wave that is in the opposite direction, and thus decreasing the QRS-wave height [49] and preventing the algorithm to properly enhance the QRS-wave amplitudes before detection. A comparison of the QRS-wave detection performance with the most cited [13], [14], [45], [46], [50], [51] and recent [41], [52]–[58] QRS detectors reporting MIT-BIH Arrhythmia database results is given in Table III. The achieved $+P$ and $F1$ is better than all algorithms and Se is better than all algorithms except [59] (underlined).

QRS-wave detection performance and the comparison with the state-of-the-art QRS detectors reporting results from the QT database are given in Table IV. The proposed algorithm achieves 99.99% average Se and 99.99% average $+P$ on 105 15-minute ECG recordings and outperforms all of the algorithms.

The QRS-wave detection performance and the comparison with the state-of-the-art QRS detectors on the EDB database are given in Table V. The proposed algorithm achieves an average Se of 99.93% and an average $+P$ of 99.97% on 90 120-minute ECG recordings. Compared with the prior art, the achieved Se value is better than all and $+P$ is better than all except [60] (underlined).

TABLE VI
QRS DETECTION COMPARISON ON THE RECORDINGS 118E12 AND 118E00 OF THE MIT-BIH NST DATABASE

	QRS detection method	Se (%)	+P (%)	F1 Score (%)
This work	***Stochastic Resonance***	***99.61/ 99.78***	***100/ 99.83***	***99.81/ 99.8***
Physionet [65] [1]	GQRS	96.58/ 82.77	84.36/ 62.7	90.05/ 71.35
Pan, 1985 [45] [1]	PT	83.05/ 20.48	94.92/ 59.81	88.44/ 30.49
Martinez, 2004 [50] [1]	WT	91.72/ 82.01	77.65/ 65.36	84.09/ 72.74
Xiang, 2018 [62] [1]	CNN	94.19/ 77.32	94.44/ 72.12	94.18/ 70.36
Chandra, 2019 [39] [1]	CNN	98.68/ 88.22	90.89/ 71.37	94.6/ 78.9
Merah, 2015 [14]	Stationary WT	99.56/ 92.41	98.82/ 90.27	99.18/ 91.23
Rahul, 2021b [56]	Third power + AT	97.49/ 91	98.27/ 93.54	97.87/ 92.25

[1] Implemented in [17]. AT: Adaptive Thresholding. In each row the first result is for the recording 118e12 and the second is for the 118e00.

TABLE VII
QRS DETECTION PERFORMANCE EVALUATION OF THE PROPOSED ALGORITHM ON THE MIT-BIH NST DATABASE

ECG record #	*Total # of beats*	*Se (%)*	*+P (%)*	*F1 Score (%)*
118e24	2278	99.65	100	99.83
118e18	2278	99.61	100	99.81
118e12	2278	99.61	100	99.81
118e06	2278	99.56	99.92	99.74
118e00	2278	99.78	99.83	99.8
118e_6	2278	99.48	99.69	99.58
119e24	1987	100	100	100
119e18	1987	100	100	100
119e12	1987	99.1	99.85	99.47
119e06	1987	98.49	98.39	98.44
119e00	1987	99.5	96.44	97.95
119e_6	1987	89.02	95.21	92.01
Overall	**25590**	**98.65**	**99.11**	**98.87**

TABLE VIII
QRS DETECTION COMPARISON ON THE MIT-BIH NST DATABASE

	QRS detection method	Se (%)	+P (%)	F1 Score (%)
This work	***Stochastic Resonance***	***98.65***	***99.11***	***98.87***
Benitez, 2000 [66]	Hilbert Transform	93.48	90.6	92.02
Khamis, 2016 [13]	UNSW	93.14	86.23	89.55
Pan, 1985 [45] [1]	PT	93.15	81.83	87.12
GR, 2015 [67] [1]	GR	91.6	86.36	88.9
Merah, 2015 [14]	Stationary WT	95.3	93.98	94.63
Jia, 2020 [15]	CNN	*99.25*	96.31	97.76
Elgendi, 2013 [46]	Squaring + MA	95.39	90.25	92.74
Pander, 2022 [41]	FCMC	95.27	94.7	94.98
Rahul, 2021b [56]	Third power + AT	97.58	96.04	96.8

[1] Implemented in [13]. GR: Gutierrez Rivas algorithm, MA: Moving Average, FCMC: Fuzzy c-median Clustering, EMD: Empirical Mode Decomposition, AT: Adaptive Thresholding.

Additionally, the QRS detection performance of the algorithm is evaluated in noisy ECG recordings of the MIT-BIH NST database. For recordings with SNR values of 12 dB (recording 118e12) and 0 dB (recording 118e00) in the MIT-

BIH NST database, detection performances of the algorithm are presented in Table VI, which also presents the performances of other algorithms for the corresponding recordings. The results for all recordings in the database and a comparison of the performance with other QRS detectors are presented in Tables VII and VIII. In all twelve 30-minute noisy ECG recordings of the database, the proposed algorithm achieves an average *Se* of 98.65% and $+P$ of 99.11%, and thus a better $F1$ than all other algorithms.

Finally, the computational complexity of the proposed algorithm is investigated since the complexity is one of the metrics affecting the applicability of the algorithm in real-time heart rate monitoring applications (e.g., wearables) using ECG. Overall, the complexity increases linearly with the data length. More specifically, referring to the pseudocode in Algorithm 1, calling the PS function and assignment of the optimized parameters in line 2 add $3420n + 47134$ units of operation. Calling the SR with optimized parameters and assignment of $x(t)$ in line 3 add $71n - 69$ units of operation. Applying constant threshold by calling the TH function on $s_{out,HPF}(t)$ and assignment of the $QRS_{detected}$ in line 5 add $50n + 2$ units of operation. Obtaining performance metrics and detection performance by calling PM and DP functions and assignment of metrics in lines 6 and 7 add 33841 units of operation. The complexity of band pass and high pass filters are $6n + 65$ units of operation each. In total, the complete QRS-wave detection algorithm consists of $3553n + 81038$ units of operation where n is the total number of samples of a signal, and thus achieving $O(n)$ complexity in $Big\ Oh$ notation. Accordingly, in terms of computation time, the proposed algorithm achieves a low average computation time of 0.3435±0.0026 s per recording of the MIT-BIH Arrhythmia database using a PC with Intel(R) Core(TM) i7-8750H CPU @ 2.20 GHz and 16.0 GB of RAM with 1 TB SSD. In another system with a slightly different configuration of Intel(R) Core(TM) i5-7500 CPU @ 3.4 GHz and 16.0 GB of RAM with 1 TB HDD, the average computation time per the same recording is similar (0.3992±0.0084 s).

IV. Discussion

The analyses using individual noise types and a combined version of different noise types in Fig. 6 reveal that the proposed algorithm improves the SNR of QRS features as high as 89 dB (*em*+*ma*+*bw* noise). Furthermore, even for high noise intensities, an SNR improvement ($\Delta SNR_{detected}$) of 32 dB can be obtained (*em*+*ma*+*bw* noise).

Additionally, the algorithm facilitates the existing noise in the recordings to improve the SNR, a result that holds for all three noise types as well as their combination. However, there is an optimum noise level, where the SNR improvement is maximized, and thus verifying the SR facilitation. As the noise intensity is increased past the optimum level, the noise starts swamping the ECG signal. For the *em,* the SNR improvement peaks when the standard deviation is 0.146, whereas for the other noise types the optimum noise standard deviations are 0.096 for *ma*, 0.233 for *bw*, and 0.447 for the noise types combined.

When compared with common QRS enhancement algorithms of Pan-Tompkins [45] and Elgendi [46] in Fig. 7, the proposed algorithm achieves better SNR improvement by amounts varying between 82.9 dB ($em + ma + bw$) and 73.8 dB (em). The better SNR improvement is observed not only for the optimum em noise standard deviation of 0.146, but also even for the noise-free signal, where ΔSNR peaks for the Pan-Tompkins and the Elgendi algorithms. Finally, for the largest noise intensity tested (noise standard deviation = 0.9), the SR algorithm achieves ~28 dB greater ΔSNR than the Elgendi algorithm. It should be noted that, the significantly better SNR improvement of the proposed algorithm for small noise intensities does not translate into equally better QRS detection performance. In fact, for an em noise standard deviation of 0.219, the SR algorithm achieves an $F1$ score of 96.32% for the recording 100 of MIT-BIH Arrhythmia database; whereas the Pan-Tompkins and the Elgendi algorithms achieve $F1$ scores of 98.95% and 97.4%, respectively.

The distinguishing feature of the proposed algorithm is its better detection performance for high noise intensities. For instance, for an em noise standard deviation of 0.73, the proposed algorithm achieves 99.92% of detection sensitivity, whereas *Se* drops to 90.33% and 88.51% for the Pan-Tompkins and the Elgendi algorithms, respectively. High added noise intensities are more realistic in real life applications since ECG recording from the active subject is distorted with noise caused by activity of subject, movement of the electrodes, or muscle artifacts [10], [13], [60]. Thus, performance improvement of the proposed algorithm at high noise intensities indicates that the proposed algorithm can be used for QRS-wave detection from noisy ECG recordings.

The analysis of QRS detection performance of the proposed algorithm for varying noise intensities in Fig. 6 reveals that, unlike ΔSNR, the detection performance metrics of *Se* and $+P$ do not display the characteristic bell curve shape of the SR. Both metrics reduce with increasing noise intensity with the decrease being more substantial for $+P$ because of the increase in FP count. In fact, for all noise types, *Se* remains greater than 99.92%; whereas the $+P$ drops from 100% to 60.85% as noise standard deviation is increased from 0 to 0.9. Notably, the severity of detection performance degradation is different for different noise types. Despite the large drop in $+P$ for *em*; the $+P$ remains greater than 99.87% for all noise intensities for the *bw* noise. The poor performance for the *em* and the combination noise can be explained by the existence of features similar to characteristic QRS features in those noise types. Therefore, the number of FP is greater for these noise types as in Fig. 8(a) and Fig. 8 (d), compared to the *ma* (Fig. 8(b)) and *bw* (Fig. 8(c)).

Based on the QRS detection performance results evaluated on the MIT-BIH Arrhythmia, QT, EDB, and the NST databases, which are summarized in Tables III, IV, V, and VIII; the proposed SR algorithm outperforms all algorithms in terms of $F1$ score, which provides a balance between Se and $+P$.

The computation time and algorithm complexity of the proposed algorithm are compared with algorithms that report their complexities in Table IX. It is worth noting that computation time is dependent also on the available computation resources: Two faster algorithms use more powerful computation environments [53], [55]. However, the proposed algorithm runs faster than integrated energy [61] implementation despite being implemented on a less powerful computer.

This article has been accepted for publication in a future issue of this journal, but has not been fully edited. Content may change prior to final publication. Citation information: DOI 10.1109/JBHI.2022.3178109, IEEE Journal of Biomedical and Health Informatics

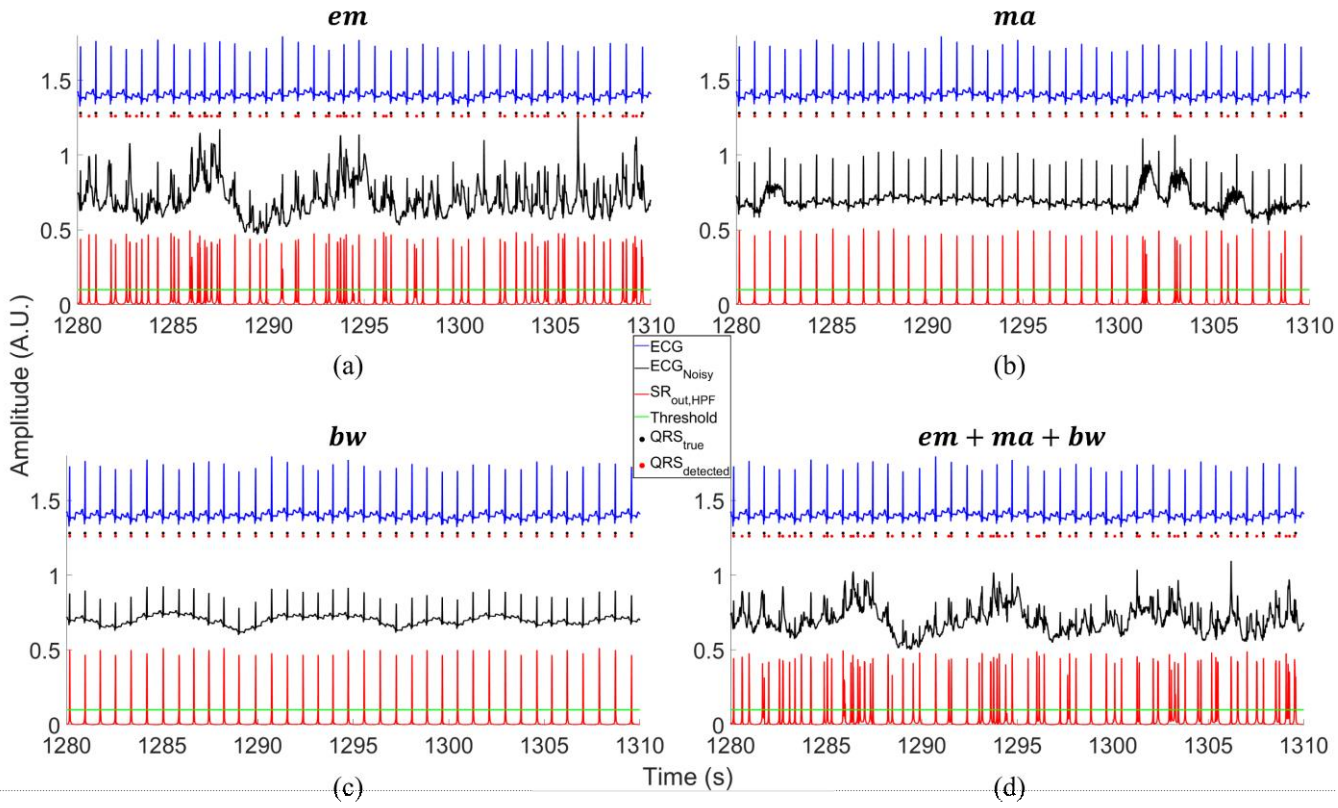

Fig. 8. Detection results of the proposed algorithm for a 30 s portion of the recording 100 of the MIT-BIH Arrhythmia database, ECG, and noise added versions of it, ECG_{noisy}; when (a) em (b) ma (c) bw, and (d) $em + ma + bw$ are individually added as in (9) with $g = 1$. The output of the QRS-Enhancement stage, $SR_{out,HPF}$, the constant threshold level, QRS_{true} (black dots) and $QRS_{detected}$ (red dots) are shown for each noise type. The signals are separated by an offset for visualization purposes. The results demonstrate the greater numbers of FPs for the em and $em + ma + bw$ cases compared to the ma and bw.

TABLE IX
COMPLEXITY COMPARISON ON THE MIT-BIH ARRHYTHMIA DATABASE

	QRS detection method	Computation time (s)	Complexity ($Big\ Oh$)
This work	***Stochastic Resonance***	***0.3435± 0.0026***	$\boldsymbol{O(n)}$
Tueche, 2021 [53]	PT-based	*0.31*	N/A
Pan, 1985 [45] [1]	PT	0.576	$O(n)$
Liu, 2019 [61]	Integrated energy	0.414	N/A
Physionet [65] [1]	JQRS	0.558	N/A
Elgendi, 2013 [46]	Squaring + MA	0.3	N/A
Xiong, 2021 [55]	Energy Segmentation	*0.22*	N/A
Xiang, 2018 [62]	CNN	14.53	$\sim O(n)$ [2]
Yuen, 2019 [17]	CNN-LSTM	N/A	$\sim O(n)$

[1] Implemented in [61], [2] $BigOh$ complexity is given in [68]. MA: Moving Average, LSTM: Long short-term memory

Based on the QRS-wave detection accuracy comparisons on four benchmarking databases (total of 14,175 minutes of recordings and over a million QRS-waves to detect) with varying difficulty levels, only three studies report slightly better performances in either Se or $+P$, but not simultaneously in both: For the MIT-BIH arrhythmia database, [59] reports better Se (+0.01%) and for the EDB database, [60] reports better $+P$ (+0.01%); while for the QT database, there are not any better algorithms than the proposed algorithm. In the NST database, [15] reports better Se (+0.6%). Compared with those methods reporting better Se or $+P$ performances, the proposed algorithm has two distinctive properties:

First, the proposed algorithm detects QRS-waves as the data streams through without running a reverse search step. Therefore, unlike [59], [60], the proposed method offers real-time QRS-detection, thereby making it more appropriate for real-time monitoring of ECG in wearable/injectable systems with limited computational resources. Second, the proposed algorithm does not need any training data for parameter optimization. On the contrary, as the authors point out in [15], the highly-complex (6-layers) convolutional neural network (CNN) is highly dependent on the training data. In fact, for the recordings 118e12 and 118e00, the proposed algorithm achieves better detection performance than all other methods including two other CNN methods [39], [62] (Table VI).

Despite achieving high SNR improvement and QRS detection performances, there are some limitations of the proposed algorithm. First, the algorithm contains several variables that need to be manually optimized before fed with a recording. On the other hand, the parameter optimization is performed based on maximization of SNR of the ECG recording calculated using only the detected QRS waves, without the need for *apriori* knowledge on the true QRS locations [32].

Second, the algorithm complexity is dominated by the parametric search step. It is important to note that, for a given dataset, optimization of all parameters is performed only once for the first recording. For each of the other recordings, the only parameter that needs to be optimized individually is h: All other parameters are held constant. The search for h introduces a

constant factor to *Big Oh* notation complexity and the complexity of the algorithm remains $O(n)$. The parametric search of h parameter increases the run time by ~5%.

Additionally, the study has one major limitation. The three noise recordings (i.e., *em, ma, bw*) used to investigate the effect of noise intensity on SNR improvement and QRS detection are static noise recordings from the MIT-BIH NST database. Although the recordings well reflect the time and frequency characteristics of three major noise sources in an actual ECG recording, further analyses could be performed on multiple noise recordings, which is left as a future study.

V. Conclusion

The study investigates a new QRS detection algorithm that enhances QRS in a nonlinear system modeling the movement of a particle inside a monostable potential-well with the x-position of the particle in the potential-well being the output. The SNR improvement with noise intensity displays the characteristic bell curve shape of stochastic resonance, which peaks at a non-zero noise intensity. Accordingly, in four benchmarking databases, the proposed algorithm outperforms all existing QRS-detection algorithms in terms of $F1$ score. Notably, the algorithm offers real-time QRS-detection and does not rely on training datasets. In a realistic ECG-based HR monitoring scenario, the proposed algorithm can detect the QRS features of a noisy recording after the algorithm parameters are optimized once and solely based on maximizing the output SNR for that recording. The future steps will be towards fully automating the parameter search step in a computationally efficient way and implementing the algorithm in a wearable ECG system to evaluate the algorithm in ECG recordings with varying noise conditions.

References

[1] J. Malcolm Arnold, D. H. Fitchett, J. G. Howlett, E. M. Lonn, and J.-C. Tardif, "Resting heart rate: A modifiable prognostic indicator of cardiovascular risk and outcomes?," *Can. J. Cardiol.*, vol. 24, pp. 3A-15A, May 2008, doi: 10.1016/S0828-282X(08)71019-5.

[2] M. Shabaan *et al.*, "Survey: smartphone-based assessment of cardiovascular diseases using ECG and PPG analysis," *BMC Med. Inform. Decis. Mak.*, vol. 20, no. 1, p. 177, Jul. 2020, doi: 10.1186/s12911-020-01199-7.

[3] J. Sztajzel, "Heart rate variability: a noninvasive electrocardiographic method to measure the autonomic nervous system," *Swiss Med. Wkly.*, vol. 134, no. 35–36, pp. 514–522, Sep. 2004, doi: 2004/35/smw-10321.

[4] K. B. Min, J.-Y. Min, D. Paek, S.-I. Cho, and M. Son, "Is 5-Minute Heart Rate Variability a Useful Measure for Monitoring the Autonomic Nervous System of Workers?," *Int. Heart. J.*, vol. 49, no. 2, pp. 175–181, 2008, doi: 10.1536/ihj.49.175.

[5] S. Evans, L. C. Seidman, J. C. Tsao, K. C. Lung, L. K. Zeltzer, and B. D. Naliboff, "Heart rate variability as a biomarker for autonomic nervous system response differences between children with chronic pain and healthy control children," *J. Pain Res.*, vol. 6, pp. 449–457, Jun. 2013, doi: 10.2147/JPR.S43849.

[6] G. B. Moody, W. Muldrow, and R. G. Mark, "The MIT-BIH Noise Stress Test Database." physionet.org, 1992. doi: 10.13026/C2HS3T.

[7] L. Sörnmo and P. Laguna, "Electrocardiogram (ECG) Signal Processing," in *Wiley Encyclopedia of Biomedical Engineering*, American Cancer Society, 2006. doi: 10.1002/9780471740360.ebs1482.

[8] I. Jekova, V. Krasteva, I. Christov, and R. Abächerli, "Threshold-based system for noise detection in multilead ECG recordings," *Physiol. Meas.*, vol. 33, no. 9, pp. 1463–1477, Aug. 2012, doi: 10.1088/0967-3334/33/9/1463.

[9] L. G. Tereshchenko and M. E. Josephson, "Frequency content and characteristics of ventricular conduction," *J. Electrocardiol.*, vol. 48, no. 6, pp. 933–937, Nov. 2015, doi: 10.1016/j.jelectrocard.2015.08.034.

[10] C. Nayak, S. K. Saha, R. Kar, and D. Mandal, "An Efficient and Robust Digital Fractional Order Differentiator Based ECG Pre-Processor Design for QRS Detection," *IEEE Trans. Biomed. Circuits Syst.*, vol. 13, no. 4, pp. 682–696, Aug. 2019, doi: 10.1109/TBCAS.2019.2916676.

[11] A. Martínez, R. Alcaraz, and J. J. Rieta, "Application of the phasor transform for automatic delineation of single-lead ECG fiducial points," *Physiol. Meas.*, vol. 31, no. 11, pp. 1467–1485, Sep. 2010, doi: 10.1088/0967-3334/31/11/005.

[12] G. B. Moody and R. G. Mark, "The impact of the MIT-BIH Arrhythmia Database," *IEEE Eng. Med. Biol. Mag.*, vol. 20, no. 3, pp. 45–50, Jun. 2001, doi: 10.1109/51.932724.

[13] H. Khamis, R. Weiss, Y. Xie, C.-W. Chang, N. H. Lovell, and S. J. Redmond, "QRS Detection Algorithm for Telehealth Electrocardiogram Recordings," *IEEE Trans. Biomed. Eng.*, vol. 63, no. 7, pp. 1377–1388, Jul. 2016, doi: 10.1109/TBME.2016.2549060.

[14] M. Merah, T. A. Abdelmalik, and B. H. Larbi, "R-peaks detection based on stationary wavelet transform," *Comput. Methods Programs Biomed.*, vol. 121, no. 3, pp. 149–160, Oct. 2015, doi: 10.1016/j.cmpb.2015.06.003.

[15] M. Jia, F. Li, J. Wu, Z. Chen, and Y. Pu, "Robust QRS Detection Using High-Resolution Wavelet Packet Decomposition and Time-Attention Convolutional Neural Network," *IEEE Access*, vol. 8, pp. 16979–16988, 2020, doi: 10.1109/ACCESS.2020.2967775.

[16] D. Pandit, L. Zhang, C. Liu, S. Chattopadhyay, N. Aslam, and C. P. Lim, "A lightweight QRS detector for single lead ECG signals using a max-min difference algorithm," *Comput. Methods Programs Biomed.*, vol. 144, pp. 61–75, Jun. 2017, doi: 10.1016/j.cmpb.2017.02.028.

[17] B. Yuen, X. Dong, and T. Lu, "Inter-Patient CNN-LSTM for QRS Complex Detection in Noisy ECG Signals," *IEEE Access*, vol. 7, pp. 169359–169370, 2019, doi: 10.1109/ACCESS.2019.2955738.

[18] L. Gammaitoni, P. Hänggi, P. Jung, and F. Marchesoni, "Stochastic resonance," *Rev. Mod. Phys.*, vol. 70, no. 1, pp. 223–287, Jan. 1998, doi: 10.1103/RevModPhys.70.223.

[19] G. Zhang, Y. Zhang, T. Zhang, and J. Xiao, "Stochastic Resonance in Second-Order Underdamped System With Exponential Bistable Potential for Bearing Fault Diagnosis," *IEEE Access*, vol. 6, pp. 42431–42444, 2018, doi: 10.1109/ACCESS.2018.2856620.

[20] H. Zhang, Q. He, and F. Kong, "Stochastic Resonance in an Underdamped System with Pinning Potential for Weak Signal Detection," *Sensors*, vol. 15, no. 9, pp. 21169–21195, Aug. 2015, doi: 10.3390/s150921169.

[21] J. Shu-Yao, Y. Fei, C. Ke-Yu, and C. En, "Application of stochastic resonance technology in underwater acoustic weak signal detection," in *OCEANS 2016 - Shanghai*, Apr. 2016, pp. 1–5. doi: 10.1109/OCEANSAP.2016.7485567.

[22] M. Kawaguchi, H. Mino, and D. M. Durand, "Stochastic Resonance Can Enhance Information Transmission in Neural Networks," *IEEE Trans. Biomed. Eng.*, vol. 58, no. 7, pp. 1950–1958, Jul. 2011, doi: 10.1109/TBME.2011.2126571.

[23] P. W. Miller, I. W. McGowan, U. Bergmann, D. Farrell, and D. F. McLaughlin, "Stochastic resonance as a proposed neurobiological model for Eye Movement Desensitization and Reprocessing (EMDR) therapy," *Med. Hypotheses*, vol. 121, pp. 106–111, Dec. 2018, doi: 10.1016/j.mehy.2018.09.010.

[24] A. Patel and B. Kosko, "Stochastic Resonance in Continuous and Spiking Neuron Models With Levy Noise," *IEEE Trans. Neural Netw.*, vol. 19, no. 12, pp. 1993–2008, Dec. 2008, doi: 10.1109/TNN.2008.2005610.

[25] S. Lu, Q. He, and F. Kong, "Effects of underdamped step-varying second-order stochastic resonance for weak signal detection," *Digit. Signal Process.*, vol. 36, pp. 93–103, Jan. 2015, doi: 10.1016/j.dsp.2014.09.014.

[26] C. López, W. Zhong, S. Lu, F. Cong, and I. Cortese, "Stochastic resonance in an underdamped system with FitzHug-Nagumo potential for weak signal detection," *J. Sound Vib.*, vol. 411, pp. 34–46, Dec. 2017, doi: 10.1016/j.jsv.2017.08.043.

[27] M. D. McDonnell and D. Abbott, "What Is Stochastic Resonance? Definitions, Misconceptions, Debates, and Its Relevance to Biology," *PLOS Comput. Biol.*, vol. 5, no. 5, p. e1000348, May 2009, doi: 10.1371/journal.pcbi.1000348.

[28] P. Zhou, S. Lu, F. Liu, Y. Liu, G. Li, and J. Zhao, "Novel synthetic index-based adaptive stochastic resonance method and its application in bearing fault diagnosis," *J. Sound Vib.*, vol. 391, pp. 194–210, Mar. 2017, doi: 10.1016/j.jsv.2016.12.017.

[29] F. Chapeau-Blondeau and X. Godivier, "Theory of stochastic resonance in signal transmission by static nonlinear systems," *Phys. Rev. E*, vol. 55, no. 2, pp. 1478–1495, Feb. 1997, doi: 10.1103/PhysRevE.55.1478.

[30] N. G. Stocks, "Information transmission in parallel threshold arrays: Suprathreshold stochastic resonance," *Phys. Rev. E*, vol. 63, no. 4, p. 041114, Mar. 2001, doi: 10.1103/PhysRevE.63.041114.

[31] C. B. Güngör and H. Töreyin, "Facilitating stochastic resonance as a pre-emphasis method for neural spike detection," *J. Neural Eng.*, vol. 17, no. 4, p. 046047, Sep. 2020, doi: 10.1088/1741-2552/abae8a.

[32] C. B. Güngör, P. P. Mercier, and H. Töreyin, "Investigating well potential parameters on neural spike enhancement in a stochastic-resonance pre-emphasis algorithm," *J. Neural Eng.*, vol. 18, no. 4, p. 046062, May 2021, doi: 10.1088/1741-2552/abfd0f.

[33] W. Zhang, P. Shi, M. Li, Y. Jiao, and D. Han, "Signal Detection Based on Second-Order Underdamped Tristable Stochastic Resonance and Its Application to Weak Fault Diagnosis," *IEEE Access*, vol. 7, pp. 173753–173765, 2019, doi: 10.1109/ACCESS.2019.2955605.

[34] H. A. Kramers, "Brownian motion in a field of force and the diffusion model of chemical reactions," *Physica*, vol. 7, no. 4, pp. 284–304, Apr. 1940, doi: 10.1016/S0031-8914(40)90098-2.

[35] J. Li and X. Pan, "A nonlinear monostable filter for bipolar pulse signal detection," *Mech. Syst. Signal Process.*, vol. 21, no. 3, pp. 1223–1232, Apr. 2007, doi: 10.1016/j.ymssp.2006.03.012.

[36] A. S. Asdi and A. H. Tewfik, "Detection of weak signals using adaptive stochastic resonance," in *1995 International Conference on Acoustics, Speech, and Signal Processing*, May 1995, vol. 2, pp. 1332–1335 vol.2. doi: 10.1109/ICASSP.1995.480486.

[37] "ANSI/AAMI EC38:1998 - Ambulatory electrocardiographs, 2ed." https://webstore.ansi.org/standards/aami/ansiaamiec381998 (accessed Aug. 15, 2021).

[38] "ANSI/AAMI EC57:1998/(R)2003 - Testing and reporting performance results of cardiac rhythm and ST segment measurement algorithms." https://webstore.ansi.org/standards/aami/ansiaamiec5719982003 (accessed Aug. 15, 2021).

[39] B. S. Chandra, C. S. Sastry, and S. Jana, "Robust Heartbeat Detection From Multimodal Data via CNN-Based Generalizable Information Fusion," *IEEE Trans. Biomed. Eng.*, vol. 66, no. 3, pp. 710–717, Mar. 2019, doi: 10.1109/TBME.2018.2854899.

[40] W. Cai and D. Hu, "QRS Complex Detection Using Novel Deep Learning Neural Networks," *IEEE Access*, vol. 8, pp. 97082–97089, 2020, doi: 10.1109/ACCESS.2020.2997473.

[41] T. Pander, "A new approach to adaptive threshold based method for QRS detection with fuzzy clustering," *Biocybern. Biomed. Eng.*, vol. 42, no. 1, pp. 404–425, Jan. 2022, doi: 10.1016/j.bbe.2022.02.007.

[42] M. Lee, D. Park, S.-Y. Dong, and I. Youn, "A Novel R Peak Detection Method for Mobile Environments," *IEEE Access*, vol. 6, pp. 51227–51237, 2018, doi: 10.1109/ACCESS.2018.2867329.

[43] P. Laguna, R. G. Mark, A. Goldberg, and G. B. Moody, "A database for evaluation of algorithms for measurement of QT and other waveform intervals in the ECG," in *Computers in Cardiology 1997*, Sep. 1997, pp. 673–676. doi: 10.1109/CIC.1997.648140.

[44] A. Taddei *et al.*, "The European ST-T database: standard for evaluating systems for the analysis of ST-T changes in ambulatory electrocardiography," *Eur. Heart J.*, vol. 13, no. 9, pp. 1164–1172, Sep. 1992, doi: 10.1093/oxfordjournals.eurheartj.a060332.

[45] J. Pan and W. J. Tompkins, "A Real-Time QRS Detection Algorithm," *IEEE Trans. Biomed. Eng.*, vol. BME-32, no. 3, pp. 230–236, Mar. 1985, doi: 10.1109/TBME.1985.325532.

[46] M. Elgendi, "Fast QRS Detection with an Optimized Knowledge-Based Method: Evaluation on 11 Standard ECG Databases," *PLOS ONE*, vol. 8, no. 9, p. e73557, Sep. 2013, doi: 10.1371/journal.pone.0073557.

[47] "Complete Pan Tompkins Implementation ECG QRS detector." https://www.mathworks.com/matlabcentral/fileexchange/45840-complete-pan-tompkins-implementation-ecg-qrs-detector (accessed Aug. 14, 2021).

[48] M. Begić, *ECG-detection-Elgendi-algorithm-Matlab*. 2021. Accessed: Aug. 14, 2021. [Online]. Available: https://github.com/Maja5556/ECG-detection-Elgendi-algorithm-Matlab

[49] "Braunwald's Heart Disease: A Textbook of Cardiovascular Medicine, Single Volume." https://www.us.elsevierhealth.com/braunwalds-heart-disease-a-textbook-of-cardiovascular-medicine-single-volume-9780323462990.html (accessed Apr. 04, 2022).

[50] J. P. Martinez, R. Almeida, S. Olmos, A. P. Rocha, and P. Laguna, "A wavelet-based ECG delineator: evaluation on standard databases," *IEEE Trans. Biomed. Eng.*, vol. 51, no. 4, pp. 570–581, Apr. 2004, doi: 10.1109/TBME.2003.821031.

[51] A. Ghaffari, M. R. Homaeinezhad, M. Akraminia, M. Atarod, and M. Daevaeiha, "A robust wavelet-based multi-lead electrocardiogram delineation algorithm," *Med. Eng. Phys.*, vol. 31, no. 10, pp. 1219–1227, Dec. 2009, doi: 10.1016/j.medengphy.2009.07.017.

[52] J. Rahul, M. Sora, and L. D. Sharma, "A novel and lightweight P, QRS, and T peaks detector using adaptive thresholding and template waveform," *Comput. Biol. Med.*, vol. 132, p. 104307, May 2021, doi: 10.1016/j.compbiomed.2021.104307.

[53] F. Tueche, Y. Mohamadou, A. Djeukam, L. C. N. Kouekeu, R. Seujip, and M. Tonka, "Embedded Algorithm for QRS Detection Based on Signal Shape," *IEEE Trans. Instrum. Meas.*, vol. 70, pp. 1–12, 2021, doi: 10.1109/TIM.2021.3051412.

[54] A. Peimankar and S. Puthusserypady, "DENS-ECG: A deep learning approach for ECG signal delineation," *Expert Syst. Appl.*, vol. 165, p. 113911, Mar. 2021, doi: 10.1016/j.eswa.2020.113911.

[55] H. Xiong, M. Liang, and J. Liu, "A Real-Time QRS Detection Algorithm Based on Energy Segmentation for Exercise Electrocardiogram," *Circuits Syst. Signal Process.*, vol. 40, no. 10, pp. 4969–4985, Oct. 2021, doi: 10.1007/s00034-021-01702-z.

[56] J. Rahul, M. Sora, and L. D. Sharma, "Dynamic thresholding based efficient QRS complex detection with low computational overhead," *Biomed. Signal Process. Control*, vol. 67, p. 102519, May 2021, doi: 10.1016/j.bspc.2021.102519.

[57] M. Lee and J.-H. Lee, "A robust fusion algorithm of LBP and IMF with recursive feature elimination-based ECG processing for QRS and arrhythmia detection," *Appl. Intell.*, vol. 52, no. 1, pp. 939–953, Jan. 2022, doi: 10.1007/s10489-021-02368-5.

[58] M. U. Zahid *et al.*, "Robust R-Peak Detection in Low-Quality Holter ECGs Using 1D Convolutional Neural Network," *IEEE Trans. Biomed. Eng.*, vol. 69, no. 1, pp. 119–128, Jan. 2022, doi: 10.1109/TBME.2021.3088218.

[59] M. B. Hossain, S. K. Bashar, A. J. Walkey, D. D. McManus, and K. H. Chon, "An Accurate QRS Complex and P Wave Detection in ECG Signals Using Complete Ensemble Empirical Mode Decomposition with Adaptive Noise Approach," *IEEE Access*, vol. 7, pp. 128869–128880, 2019, doi: 10.1109/ACCESS.2019.2939943.

[60] A. Burguera, "Fast QRS Detection and ECG Compression Based on Signal Structural Analysis," *IEEE J. Biomed. Health Inform.*, vol. 23, no. 1, pp. 123–131, Jan. 2019, doi: 10.1109/JBHI.2018.2792404.

[61] C. Liu *et al.*, "Signal Quality Assessment and Lightweight QRS Detection for Wearable ECG SmartVest System," *IEEE Internet Things J.*, vol. 6, no. 2, pp. 1363–1374, Apr. 2019, doi: 10.1109/JIOT.2018.2844090.

[62] Y. Xiang, Z. Lin, and J. Meng, "Automatic QRS complex detection using two-level convolutional neural network," *Biomed. Eng. OnLine*, vol. 17, p. 13, Jan. 2018, doi: 10.1186/s12938-018-0441-4.

[63] A. Chen *et al.*, "A Real Time QRS Detection Algorithm Based on ET and PD Controlled Threshold Strategy," *Sensors*, vol. 20, no. 14, p. 4003, Jul. 2020, doi: 10.3390/s20144003.

[64] S. Modak, L. Y. Taha, and E. Abdel-Raheem, "A Novel Method of QRS Detection Using Time and Amplitude Thresholds With Statistical False Peak Elimination," *IEEE Access*, vol. 9, pp. 46079–46092, 2021, doi: 10.1109/ACCESS.2021.3067179.

[65] "PhysioNet Software." https://physionet.org/about/software/ (accessed Oct. 01, 2021).

[66] D. S. Benitez, P. A. Gaydecki, A. Zaidi, and A. P. Fitzpatrick, "A new QRS detection algorithm based on the Hilbert transform," in *Computers in Cardiology 2000. Vol.27 (Cat. 00CH37163)*, Sep. 2000, pp. 379–382. doi: 10.1109/CIC.2000.898536.

[67] R. Gutiérrez-Rivas, J. J. García, W. P. Marnane, and Á. Hernández, "Novel Real-Time Low-Complexity QRS Complex Detector Based on Adaptive Thresholding," *IEEE Sens. J.*, vol. 15, no. 10, pp. 6036–6043, Oct. 2015, doi: 10.1109/JSEN.2015.2450773.

[68] S. Sakib, M. M. Fouda, Z. Md. Fadlullah, N. Nasser, and W. Alasmary, "A Proof-of-Concept of Ultra-Edge Smart IoT Sensor: A Continuous and Lightweight Arrhythmia Monitoring Approach," *IEEE Access*, vol. 9, pp. 26093–26106, 2021, doi: 10.1109/ACCESS.2021.3056509.

[69] Ö. Yakut and E. D. Bolat, "An improved QRS complex detection method having low computational load," *Biomed. Signal Process. Control,* vol. 42, pp. 230–241, Apr. 2018, doi: 10.1016/j.bspc.2018.02.004.